Research Square

Preprints are preliminary reports that have not undergone peer review.
They should not be considered conclusive, used to inform clinical practice,
or referenced by the media as validated information.

Discovering Small-Molecule WEE1 Binders through Iterative Virtual Screening

Paola Moyano-Gómez
University of Turku
Pekka Roivas
University of Turku
Veera Soininen
University of Turku
Roosa Saarimaa
University of Turku
Sanna Niinivehmas
University of Turku
Ulla Pentikäinen
University of Turku
Olli T. Pentikäinen
pentikai@utu.fi

University of Turku

Research Article

Keywords: WEE1, ligand binding, pharmacophore modeling, virtual screening, molecular docking

Posted Date: November 12th, 2026

DOI: https://doi.org/10.21203/rs.3.rs-11388804/v1

License: This work is licensed under a Creative Commons Attribution 4.0 International License.
Read Full License

Additional Declarations: No competing interests reported.

Discovering Small-Molecule WEE1 Binders through Iterative Virtual Screening

Paola Moyano-Gómez[1,2], Pekka Roivas[1,3], Veera Soininen[1,2], Roosa Saarimaa[1,2], Sanna Niinivehmas[1,2,4], Ulla Pentikäinen[1,3], Olli T. Pentikäinen[1,2,4,*]

[1]Institute of Biomedicine, Integrative Physiology and Pharmacology, University of Turku, 20014, Turku, Finland
[2]InFLAMES Research Flagship, University of Turku, 20014, Turku, Finland
[3]Turku Bioscience Centre, University of Turku, FI-20520, Turku, Finland
[4]Aurlide Ltd, Lemminkäisenkatu 14-18A, 20520, Turku, Finland

*Corresponding author: pentikai@utu.fi

ABSTRACT

Wee1-like protein kinase (WEE1) is a key regulator of the G2/M cell cycle checkpoint, preventing premature mitosis by phosphorylating cyclin-dependent kinase 1 (CDK1) and allowing time for DNA repair before division. Small-molecule Wee1 inhibitors are being investigated as a way to induce mitotic failure in cancer cells. Although several WEE1 inhibitors have entered clinical trials (phases I/II), none has received regulatory approval, underscoring the need for more selective and effective compounds. Here, complementary virtual screening strategies were used to identify novel small-molecule binders of WEE1. Structure-based screening of the ATP-binding pocket, combining docking, pharmacophore modeling, pose filtering, and evaluation of two protein structures, selected compounds for experimental testing. Microscale thermophoresis (MST) detected binding for 65 of 115 tested compounds (57%); ten had dissociation constants below 10 μM. These relatively small compounds (267–399 g/mol) are structurally distinct from known WEE1 inhibitors and provide starting points for future optimization.

Keywords:

WEE1, ligand binding, pharmacophore modeling, virtual screening, molecular docking

1. INTRODUCTION

Wee1-like protein kinase (WEE1) is a member of the serine-threonine kinase family involved in mitosis entry. It works alongside the membrane-associated tyrosine-and threonine-specific cdc2-inhibitory kinase (PKMYT1) and another WEE1 kinase, WEE1b. These kinases share sequence similarity in their kinase domains but differ in regulation, temporal expression, and localization. WEE1, located in the nucleus, prevents premature entry into mitosis by halting the cell cycle in S phase to allow DNA damage repair through phosphorylation of the cyclin-dependent kinase 1 (CDK1)-Cyclin B complex [1, 2].

CDK1 binds cyclin B during cell cycle progression to form an active heterodimer that facilitates the transition from the G2 phase to the M phase. When DNA damage occurs, the ataxia-telangiectasia-related (ATR) signaling pathway is activated [3], leading to the phosphorylation of WEE1, which then phosphorylates tyrosine 15 (Y15) of CDK1. As WEE1 levels decrease, the CDK1-cyclin B complex promotes the phosphorylation of WEE1 kinase. This disruption in the balance between WEE1 and the CDK1-cyclin B complex marks the kinase for proteolytic degradation, ultimately resulting in the inactivation of WEE1 [2, 4].

Cancer cells often have defective DNA repair, making them highly reliant on the G2/M checkpoint for survival. For example, tumors with mutations in the p53 gene lose control of the G1 checkpoint, increasing their dependence on the G2 checkpoint [5, 6]. This checkpoint is regulated by the kinase WEE1, which is elevated in cancer cells. Research has shown that inhibiting WEE1 causes cancer cells to enter mitosis prematurely, before repairing DNA damage, leading to mitotic catastrophe and cell death. This strategy is known as synthetic lethality, in which blocking a compensatory mechanism in cancer cells causes their death while leaving normal cells unaffected [2, 7, 8].

Structurally, the design of WEE1 inhibitors has focused on the ATP-binding pocket within the kinase domain, where crystallographic insights highlight the hinge and hydrophobic binding regions that guide molecular design. ATP interactions have served as anchoring points for developing heteroaromatic scaffolds and for making modifications that enhance selectivity. Generally, the identified WEE1 inhibitors [4, 9] can be classified into six chemical series based on their scaffolds (Fig. 1): pyrrolocarbazoles, pyridopyrimidines, pyrazolopyrimidinones, pyrimidine-based tricyclics, pyrrolopyrimidines, and pyrimidopyrimidines.

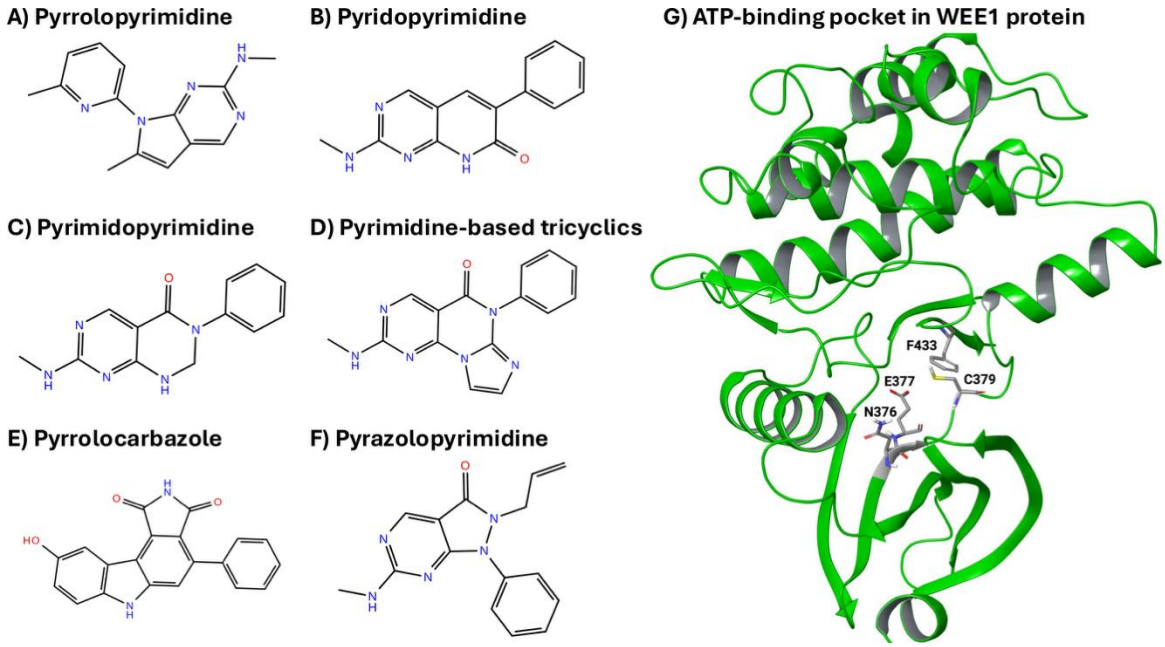


Fig. 1 Representative scaffolds of WEE1 inhibitors and the ATP-binding pocket of the WEE1 kinase. Two-dimensional structures of selected WEE1 inhibitors are shown, classified into six core scaffolds (A–F), highlighting the structural diversity of known chemotypes. The ATP-binding pocket (G) of the WEE1 kinase (PDB: 8BJU [3]) is shown with key interacting residues—C379, E377, N376, and F433—shown as grey sticks within the green-colored secondary structural framework.

Although no WEE1 inhibitors are currently approved because of persistent efficacy and toxicity concerns [2, 6, 7, 10], substantial progress has been made in inhibitor discovery and development. This effort was initiated by the pyrazolopyrimidine Adavosertib (AZD1775) (Fig. 2A), which provided proof of concept but was limited by clinical challenges. More recently, second-generation compounds, including Azenosertib (ZN-c3) (Fig. 2B), Zedoresertib (Debio 0123) (Fig. 2C), and Potrasertib (IMP7068) (Fig. 2D), have entered active clinical evaluation [11–14]. However, none of these investigational agents has received FDA approval, and target-mediated toxicities, including gastrointestinal adverse effects and transient hematologic events, remain a concern. Although Azenosertib and related compounds are intended to minimize off-target activity, broad kinome profiling indicates that achieving complete active-site selectivity remains difficult [9, 15–18]. Accordingly, refining intermittent dosing strategies and developing more selective small-molecule WEE1 inhibitors remain key objectives.

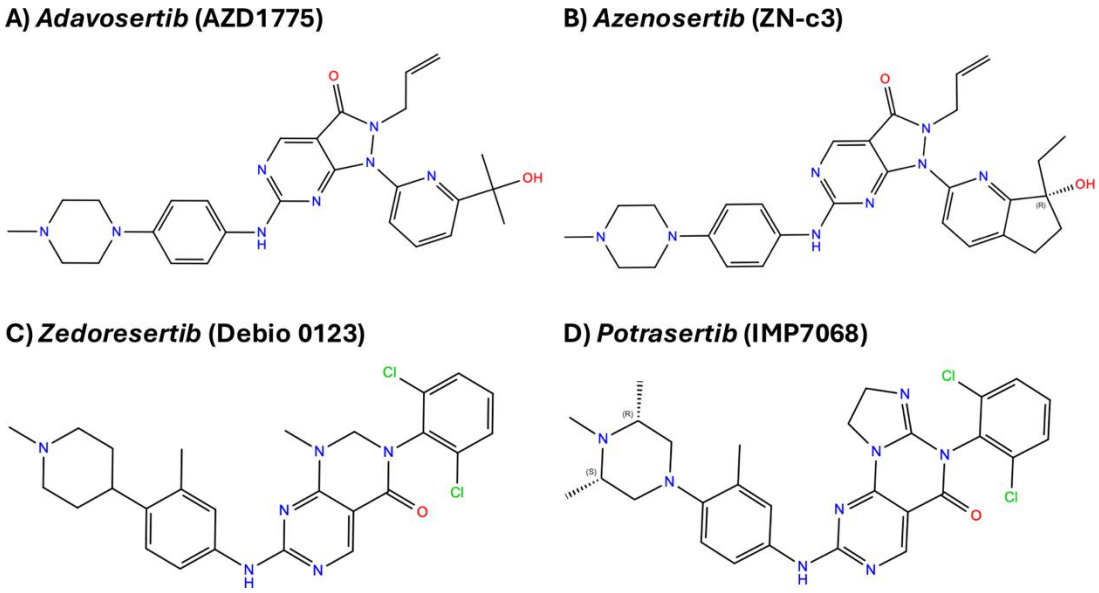


Fig. 2 Chemical structures of representative WEE1 inhibitors evaluated in clinical trials. Two-dimensional structures of WEE1 inhibitors that have entered clinical evaluation are shown: (A) Adavosertib (AZD1775), (B) Azenosertib (ZN-c3), (C) Zenoresertib (Debio 0123), and (D) Potrasertib (IMP7068) [11–14].

With several co-crystallized structures of the WEE1 kinase domain available [6, 9], we used a multi-stage virtual screening strategy to identify candidate binders from commercial compound libraries. The initial structure-based screen combined docking against two WEE1 structures with pharmacophore rescoring and interaction-based pose filtering. Experimental binding results subsequently guided a substructure search based on the strongest binders identified in batch number two and batch number three. Microscale Thermophoresis (MST) identified WEE1-binding compounds, which are termed binders.

2. MATERIALS AND METHODS

2.1. Protein Preparation

The three-dimensional (3D) X-ray co-crystallized protein structures, PDB IDs 5VC3 [10] and 8BJU [3], were retrieved from the RCSB Protein Data Bank [19]. Both structures were protonated using REDUCE v3.24 [20], and all water molecules and co-crystallized ligands were removed before further processing. For pharmacophore modeling, only the 5VC3 structure was used. This protein was prepared using the Protein Preparation Wizard in MAESTRO 2023-3 [21]. To facilitate structural comparisons of the protein structures and docked small molecules, the 5VC3 and 8BJU structures were superposed using VERTAA within the Bodil Modeling environment [22].

2.2. Small-Molecule Preparation

The SPECS commercial database was initially compiled from the July 2022 set (accession date: 12July2022; 202,761 compounds) and later updated with the April 2026 set (accession date: 05April2026; 330,020 compounds). The Enamine collection comprised 4,573,375 compounds from April 2026 (accession date: 05April2026). All sets were filtered with DataWarrior v6.1.0 [23] according to the following criteria: a molecular weight of 250-550 g/mol, no more than nine rotatable bonds, and a calculated partition coefficient between octanol and water (cLogP) of ≤ 5.7. This resulted in 141,078 and 237,923 compounds for the SPEC sets, July 2022 and

April 2026, respectively, and 3,77,943 compounds from Enamine. The active WEE1 compound set for pharmacophore modeling was obtained from DUD-E (Database of Useful Decoys–Enhanced) [24]. All small molecule libraries were prepared with the LigPrep module in MAESTRO 2023-3 [25], using the OPLS3 force field [26] at pH 7.4.

2.3. Flexible Molecular Docking

A docking box with a 10 Å radius around the centroid of the co-crystallized ligand was defined within the protein structure. Molecular docking was then performed using PLANTS v1.2 [27], applying the software's default settings for speed 1.

2.4. Pharmacophore Modeling

The pharmacophore model was constructed using docked active compounds from the DUD-E (Directory of Useful Decoys, Enhanced) dataset [24]. Compounds were categorized as active if their IC_{50} values were below 990 nM, while the remaining were considered inactive. Pharmacophore modeling was performed using the PHASE module in MAESTRO 2023-3 [28], aiming to capture at least 70% of the active compounds and incorporating between 4 and 7 features in the generated hypothesis. The resulting pharmacophore model was subsequently used to rescore the docked conformations of the commercial dataset from batch number one**.**

2.5. Similarity two- and three-dimensional search

The four strongest binders from the structure-based screen in batch number one served as reference compounds to expand the search for analogs and substructures in batch number two. This search covered compounds from SPECS and Enamine, the March 2026 and April 2026 sets, respectively, as well as web-based searches of both databases. Using the ShaEP method [29], candidates were identified with a shape/electrostatic potential (ESP) score of 0.75 or higher, and the same threshold was applied to filter web search results. To remove duplicates, results from both sources were merged to retain a unique set of compounds for virtual screening in batch number two. For batch number three, the three strongest binders identified in batch number two were used as reference compounds for a substructure search of the latest SPECS dataset.

2.6. Pose Filter with Maestro

The docking poses generated by PLANTS, selected based on pharmacophore modeling from batch number 1, were refined using the *pose_filter.py* script or the Pose Filter tool in the MAESTRO2023-3 [21] suite. The same tool was used to refine the poses generated in batch number two. From batch number one, for 5VC3, poses were filtered based on the potential to form hydrogen bonds with E377 and C379, resulting in the selection of 4,610 docked conformations. For 8BJU, the filtering criteria included hydrogen bonding with C379 and N376, yielding 28,605 docked conformations. For batch number two, the filtered docking poses that formed hydrogen bonds with C379 and N376 using the 8BJU protein were 24,733 for both SPECS and Enamine. All filtered poses were then ranked by their PLANTS docking scores, and the top two-scoring conformations for each target were extracted for visualization.

2.7. Biochemical assays

The binding of the selected compounds to WEE1 kinases was determined with MST technology using the Monolith NT Automated MST instrument (Nanotemper Technologies). The His-tagged recombinant human WEE1 protein was purchased from MedChemTronica (Cat# HY-P701727). The protein was diluted in an assay buffer, 50 mM HEPES, 200 mM NaCl, and 1 mM Dithiothreitol at pH 7.5. A total of 115 commercially sourced compounds were tested across three batches comprising 59, 33, and 23 compounds, respectively, and were dissolved in dimethyl sulfoxide (DMSO) to prepare 5 mM solutions. For MST measurements, the WEE1 protein was labeled with fluorescent dye using His-Tag Labeling Kit RED-tris-NT (Cat# NT-L118, NanoTemper Technologies) according to the manufacturer´s instructions. Initially, all compounds were screened for potential binding using the Binding Check mode of the Monolith NT Automated instrument. Single concentrations of the molecule (250 μM) and protein (50 nM) in assay buffer supplemented with 0.05% TWEEN-20 were used. For those molecules that showed detectable binding with the WEE1 protein, K_d values were determined. A twofold dilution series of the compounds was mixed with the labeled WEE1 protein. The final compound concentrations ranged from 50 nM to 250 μM, with a final DMSO concentration of 5% in the assay buffer. The concentration of the labeled WEE1 protein was constant at 50 nM, in the experiments. The compounds that produced saturating binding curves were further evaluated in triplicate to confirm reproducibility. Monolith NT. Automated capillary chips (Cat# MO-AK002, Nanotemper Technologies) were used in all MST measurements. Normalized MST responses were fitted by nonlinear regression using the One–Site–Specific Binding model in GraphPad Prism v10.4.1[30] to estimate equilibrium dissociation constants (K_d).

2.8. Fingerprint-based structural similarity analysis

Structural similarity was assessed for the ten most promising commercial compounds ($K_d < 10$ μM) against four reference WEE1 inhibitors (Fig. 2) as well as the DUD-E active compounds used for pharmacophore modeling. Molecular structures were prepared using RDKit v2026.03.06 [31] through sanitization, parent-fragment selection, and neutralization of neutralizable charges. No additional canonical tautomer standardization was performed. Morgan fingerprints were generated using a radius of 2 and a length of 2,048 bits, with chirality excluded. Pairwise Tanimoto coefficients were calculated between each commercial compound and each reference WEE1 inhibitor structure. For the DUD-E comparison, the maximum, the minimum, and mean coefficients were calculated for each commercial compound, and the DUD-E compound with the maximum coefficient was recorded as its closest structural match.

2.9. Figure Preparation

The figures were generated using MAESTRO2023-3 [21], MAESTRO2025-1 [32], and the BODIL Modeling Environment [22].

3. RESULTS

3.1. Structure-based screening and compound selection

In this study, docking, pharmacophore modeling, pose filtering, similarity searching, and substructure searching were applied at complementary stages to prioritize compounds for experimental binding measurements. This computational workflow generated candidate binders, which were subsequently evaluated for binding to WEE1 using microscale thermophoresis (MST).

The first structure-based screening strategy involved docking active ligands from the DUD-E dataset and commercially available compounds against two WEE1 crystal structures. A pharmacophore model was then generated from DUD-E actives docked to 5VC3 (Fig. 3) and used to prioritize commercial compounds according to their predicted ligand–target interactions.

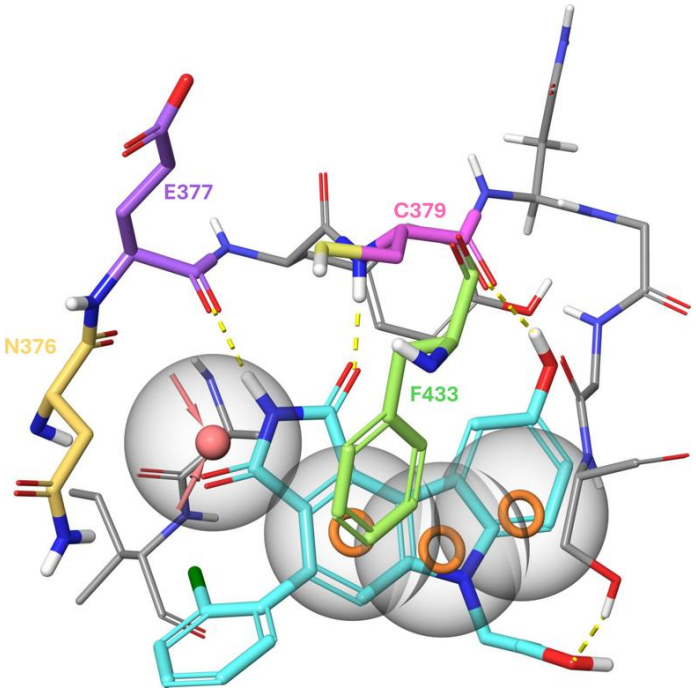


Fig. 3 Pharmacophore model of active WEE1 compounds highlighting key interactions in the ATP-binding pocket. The pharmacophore model was generated using PHASE [28] based on active WEE1 compounds in the DUD-E dataset (A database of useful Decoys–Enhanced) [24] and the 5VC3 crystal structure of WEE1[10]. The pharmacophore consists of four key features: one hydrogen bond acceptor (red sphere with two arrows) and three aromatic rings (orange rings). CHEMBL411662 (blue sticks) forms hydrogen bonds (yellow dashed lines) with C379 (pink sticks) and E377 (violet sticks) and is positioned near N376 (light orange sticks) and F433 (green sticks). This model was developed to identify key interactions critical for WEE1 inhibition.

However, the designated hydrogen-bond acceptor site in the pharmacophore model did not align optimally with E377 and did not capture a direct interaction with C379. Consequently, the docked poses were filtered using the Pose Filter tool in the MAESTRO package, with hydrogen bonding to E377 and C379 specified as filtering criteria within the 5VC3 structure. This refinement yielded 4,610 docked poses that met the defined interaction requirements. Because of the large number of retained poses, compounds were ranked according to docking scores, and up to two top-ranked conformations per compound were selected for three-dimensional visualization. This workflow ultimately led to selecting 25 commercial compounds from the SPECS library for experimental validation.

Inspection of the ATP-binding pocket in 5VC3 revealed that N376 was not oriented toward the pocket in a conformation conducive to direct hydrogen bonding (Fig. 4). Therefore, an alternative WEE1 crystal structure, 8BJU, which features a more favorable N376 conformation, was also evaluated. The same docking and pose-filtering strategy used for 5VC3 was applied to 8BJU, with filtering criteria requiring hydrogen-bond formation

with N376 and C379. Given the large number of resulting poses, compounds were again ranked by docking score, and the two highest-ranked conformations per compound were selected for three-dimensional visualization. This structure-guided approach ultimately resulted in the selection of 34 commercial compounds from the SPECS library for experimental testing.

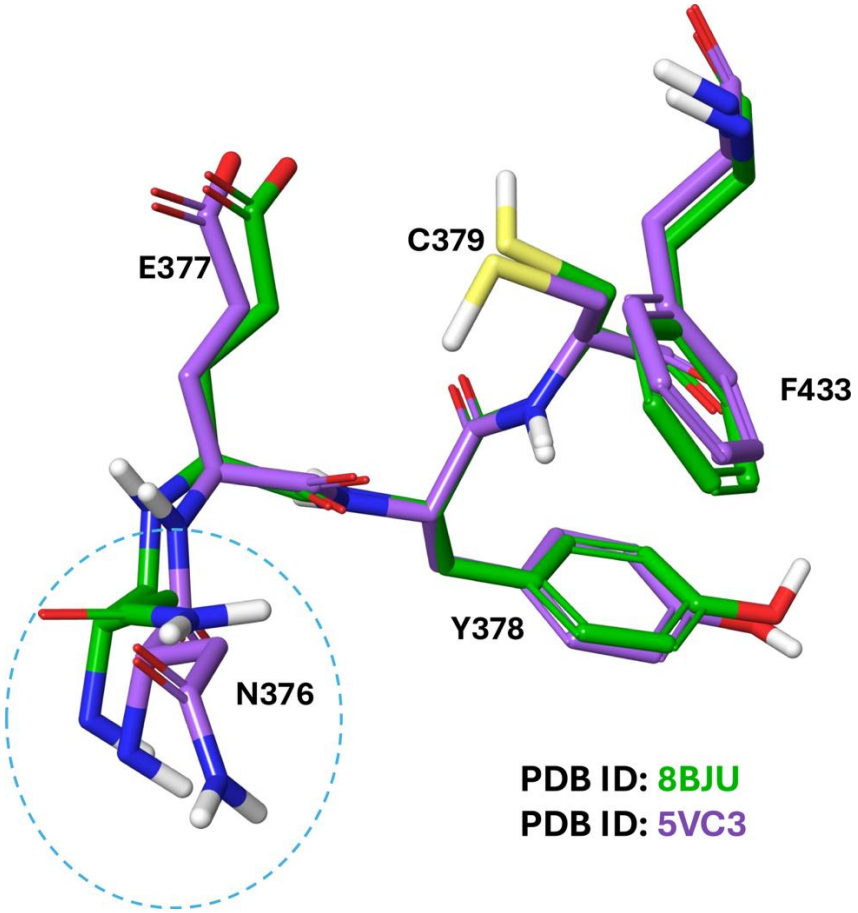


Fig. 4 Structural alignment of WEE1 ATP-Binding pockets reveals conformational variability in N376. The ATP-binding pockets of WEE1 crystal structures PDB ID 5VC3 [10] (purple sticks) and 8BJU [3] (green sticks) were aligned to assess binding site flexibility and conformational differences relevant to ligand binding. Notably, a positional shift in N376 (blue dashed circle) was observed, which may affect hydrogen bonding interactions, ligand recognition, and potentially contribute to subtype selectivity.

3.2. Experimental binding measurements

Across all batches, microscale thermophoresis (MST) measurements identified binding to WEE1 for 65 of the 115 commercially sourced compounds tested (56.5%; Table S1). Thirteen compounds exhibited K_d values below 50 µM, including ten with K_d values below 10 µM (Table 1 and Fig. 5).

Table 1. Binding dissociation constants (K_d), molecular weight (MW), logP and selection batch of the most promising commercial compounds.

Code	1	5	31	35	63	82	83	94	95	103
K_d (µM)	4	7.3	5.1	6	2.1	1.6	1.7	5	2.1	3

MW (g/mol)	348.4	267.3	307.4	290.3	398.2	360.4	296.3	358.4	387.4	324.4
logP	3	1.3	5.2	4.2	4.9	3.7	3.4	4.8	3.6	4.3
Batch	1	1	1	1	2	2	2	3	3	3

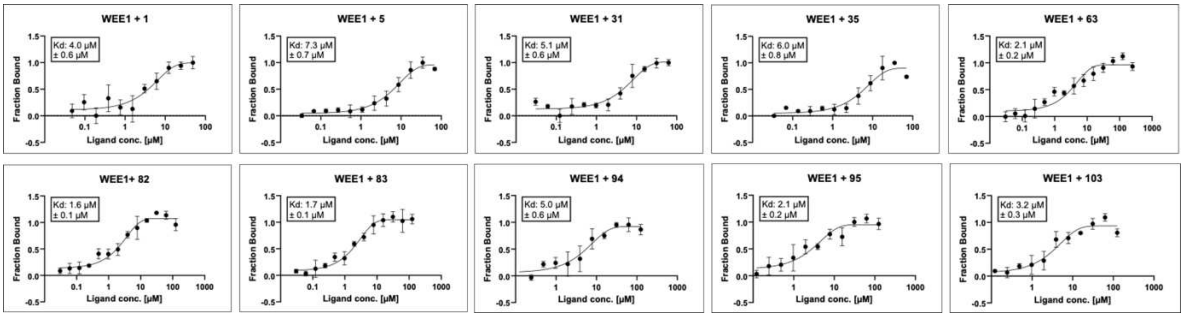


Fig. 5. MST binding curves for the ten compounds with Kd < 10 µM for WEE1. Compounds were titrated against a constant concentration of fluorescently labeled WEE1, and normalized MST responses were fitted to estimate dissociation constants (K_d). Each plot shows the fitted K_d and its standard error. Plots were generated using GraphPad Prism v10.4.1 [30].

Batch number one comprised 59 compounds prioritized through structure-based docking to 5VC3 and 8BJU, pharmacophore rescoring, and interaction-based pose filtering. Six compounds had K_d values below 50 µM, including four with K_d values below 10 µM (compounds 1, 5, 31, and 35; Table 1 and Fig. 5).

In batch number two, the four binders from batch number one were used as queries for shape- and electrostatic-similarity searches, including searches of the SPECS and Enamine collections. Of 33 compounds tested, three exhibited K_d values below 3 µM (compounds 63, 82, and 83; Table 1 and Fig. 5).

Batch number three used the three strongest batch number two binders to guide a substructure search. Of the 23 compounds tested, four showed measurable binding, and three had K_d values of 5 µM or lower (compounds 94, 95, and 103; Table 1 and Fig. 5).

3.4. Predicted ligand-protein interactions

Docked poses for compounds with experimentally determined K_d values below 50 µM were predicted to form hydrogen bonds with C379 and/or E377, frequently in conjunction with N376 (Fig. 6). Several compounds exhibiting low-micromolar binding affinity were also predicted to engage in π-stacking interactions with F433.

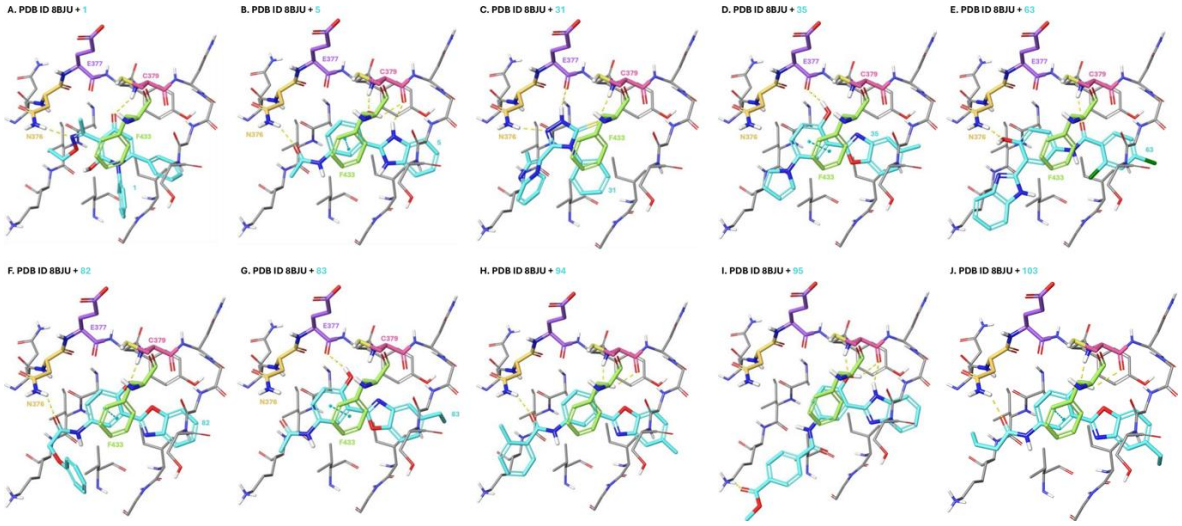


Fig. 6 Two- and three-dimensional interactions of the ten compounds with the WEE1 ATP-binding pocket. The interactions of the ten compounds (A-K) with measurable K_d values (blue sticks) and key amino acids in the ATP-binding pocket are illustrated in three-dimensional (3D) representations. The principal interacting residues are N376 (light orange sticks), E377 (violet sticks), C379 (pink sticks), and F433 (green sticks). Hydrogen bonds are depicted as yellow dashed lines, whereas π-π stacking interactions are shown as blue dashed lines. These interactions, based on the angle preferences from MAESTRO2025-1 [32], highlight the key binding features that contribute to the affinity of the selected compounds for WEE1.

3.3. Structural similarity and physicochemical properties

The ten most promising commercial compounds (Table 1) were evaluated against four reference WEE1 inhibitors (Fig. 2) and the DUD-E active compounds used for pharmacophore modeling. Morgan fingerprint-based Tanimoto similarities to the reference WEE1 inhibitors were consistently low (< 0.20), with the highest similarity of 0.170 observed between compound 94 (Fig. 6H) and Zedoresertib (Fig. 2C; Table S2). Similarities to the DUD-E active set were similarly limited, with the maximum coefficients per compound ranging from 0.155 to 0.250. The highest value was observed for compound 82 (Fig. 6F) against CHEMBL369296 (Table S3).

4. DISCUSSION

This study identified low-micromolar WEE1-binding compounds through an iterative workflow that combined structure-based virtual screening with experimentally guided follow-up searches. Among the 115 tested compounds, ten exhibited MST-derived K_d values below 10 µM. The principal contribution of this work is the identification of binding hits for further chemical exploration and the demonstration that experimentally measured binding can guide subsequent compound selection. These findings establish binding to WEE1, whereas the effects of the compounds on kinase activity remain to be determined.

The three screening rounds served complementary purposes. The initial structure-based screen combined docking, pharmacophore rescoring, and interaction-based pose filtering, yielding four binders with K_d values below 10 µM among 59 tested compounds for batch number one. Shape- and electrostatic-similarity searches seeded with these binders informed the selection of 33 compounds for batch number two. Three of these compounds exhibited K_d

values below 3 μM. The final substructure search, in batch number three, yielded three compounds with K_d values of 5 μM or lower among 23 tested compounds. These results support the practical value of using experimentally confirmed binders to focus follow-up searches. However, the screening rounds differed in their selection criteria and sampled chemical space, precluding a controlled comparison of their performance. The final round expanded the set of low-micromolar binders but did not improve upon the strongest affinity observed in batch number two.

The structure-based selection illustrates how receptor conformation and interaction criteria influence the compounds prioritized for testing. The pharmacophore model captured aromatic features near F433 but did not adequately represent the desired hydrogen-bonding interactions with E377 and C379, thereby motivating additional pose filtering. Comparison of 5VC3 and 8BJU revealed different orientations of N376, with 8BJU providing a geometry more compatible with the specified interactions involving N376 and C379. Considering alternative binding-site conformations therefore provided complementary opportunities for compound selection. Nevertheless, the predicted contacts partly reflect the criteria imposed during screening and do not independently establish their contributions to binding affinity. Experimental characterization is required to test the proposed binding modes.

Morgan fingerprint-based Tanimoto similarity was subsequently used to assess the structural resemblance of the ten most promising commercial compounds (Table 1) to the reference WEE1 inhibitors (Fig. 2), with all compounds exhibiting similarity values below 0.20 (Table S2). The compounds also showed limited resemblance to the DUD-E active compounds used for pharmacophore modeling, with no Tanimoto score exceeding 0.250 (Table S3).

The relatively low molecular weights of the strongest-binding hits may provide scope for chemical modification during optimization. Molecular weight and lipophilicity are useful considerations when balancing affinity with solubility and permeability, but these properties alone do not establish compliance with Lipinski's Rule of Five, cellular exposure, or oral bioavailability. Further optimization should therefore evaluate physicochemical properties together with binding affinity and functional activity.

The principal limitation is that MST measurements establish binding but do not demonstrate WEE1 kinase inhibition or identify the binding site. The docked poses and predicted residue contacts remain computational hypotheses, and cellular activity and kinase selectivity were not assessed. Follow-up studies should confirm binding using an independent assay, determine the effects on WEE1 kinase activity, and investigate the proposed binding modes. Together with focused analogue synthesis and selectivity profiling, these studies would establish whether the identified binding hits can be developed into WEE1 inhibitors.

5. CONCLUSIONS

This study applied complementary virtual screening strategies to identify small-molecule binders of WEE1 selected through virtual screening of the ATP-binding pocket. The initial screening in batch number one combined docking against two WEE1 crystal structures with pharmacophore modeling and interaction-based pose filtering. Experimental binding data then guided shape- and electrostatic-similarity searches, supporting compound selection for batch number two. Finally, a substructure search based on the strongest batch number two binders informed the selection of batch number three. MST detected binding to WEE1 for 65 of the 115 tested compounds. Thirteen compounds had K_d values below 50 μM, including ten below 10 μM. Morgan fingerprint comparisons

showed that the ten most promising commercial compounds had low structural similarity to both the four reference WEE1 inhibitors and the DUD-E active compounds used for pharmacophore generation, with Tanimoto similarities below 0.20 and 0.26, respectively. Although docking predicted interactions within the ATP-binding pocket, MST did not establish the binding site or confirm the predicted residue contacts. Kinase inhibition, cellular activity, and kinase selectivity were not assessed. The identified compounds provide starting points for further investigation through kinase activity assays, experimental characterization of their binding modes, selectivity profiling, and structure–activity relationship studies.

6. AUTHOR CONTRIBUTIONS

PM-G, VS, RS: Molecular modeling; PR, RS: In vitro measurements; PM-G, SN, UP, OTP: Study design and supervision. PM-G, OTP, SN: Writing-review and editing. All authors contributed to the reading of the manuscript and approved the submission.

7. ACKNOWLEDGMENTS

The Finnish IT Center for Science (CSC) is acknowledged for generous computational resources (OTP: project nos. project_2002823, project_2002811, jyy2516, and jyy2585).

8. FUNDING

This research was funded by (1) the Novo Nordisk Foundation (OTP, Pioneer Innovator (NNF21OC0068926) and Distinguished Innovator (NNF22OC0075825) grants; UP, Pioneer Innovator (NNF22OC0076296), (2) the European Regional Development Fund (ERDF) FIND-AI/ A92111 under The Innovation and Skills in Finland 2021-2027 programme (OTP), (4) the InFLAMES University–Industry Collaboration Funding (SN), the Doctoral Programme on Drug Research and Diagnostics (PR) and the Doctoral Pilot Program in Immunology (ImmuDocs) (PM-G).

9. COMPETING INTERESTS

SN and OTP are founders and shareholders of Aurlide Ltd.

10. SUPPLEMENTARY MATERIAL

Supplementary Tables (PDF): Table S1 lists the compounds selected for the in vitro binding assay, including laboratory and commercial codes, molecular weight, logP, MST-based binding assessment, topological polar surface area (TPSA), hydrogen bond acceptors and donors, rotatable bond count, and aromatic ring count. Table S2 reports compound IDs (Lab), screening batches, and Morgan fingerprint–based Tanimoto similarities to four reference WEE1 inhibitors: Adavosertib, Azenosertib, Zedoresertib, and Potrasertib. Table S3 lists the laboratory IDs, MST-derived (K_d) values, and maximum, minimum, and mean Morgan fingerprint–based Tanimoto similarities to DUD-E active compounds, along with the ChEMBL ID of each closest match.

11. REFERENCES

1. Elbæk CR, Petrosius V, Sørensen CS (2020) WEE1 kinase limits CDK activities to safeguard DNA replication and mitotic entry. Mutation Research - Fundamental and Molecular Mechanisms of Mutagenesis 819–820

2. Esposito F, Giuffrida R, Raciti G, et al (2021) Wee1 kinase: A potential target to overcome tumor resistance to therapy. Int J Mol Sci 22:. https://doi.org/10.3390/ijms221910689

3. Guler S, DiPoto MC, Crespo A, et al (2023) Selective Wee1 Inhibitors Led to Antitumor Activity In Vitro and Correlated with Myelosuppression. ACS Med Chem Lett 14:566–576. https://doi.org/10.1021/acsmedchemlett.2c00481

4. Ma J, Liu W, Li J, et al (2025) Azenosertib Is a Potent and Selective WEE1 Kinase Inhibitor with Broad Antitumor Activity Across a Range of Solid Tumors. Mol Cancer Ther 24:1171–1185. https://doi.org/10.1158/1535-7163.MCT-24-1194

5. Tamburello M, Boldini C, Abate A, et al (2026) Pharmacological WEE1 inhibition as a strategy to overcome cisplatin resistance in non-seminoma testicular cancer: insights from preclinical models. Sci Rep 16:. https://doi.org/10.1038/s41598-025-34904-5

6. Jin T, Xu W, Chen R, et al (2023) Discovery of potential WEE1 inhibitors via hybrid virtual screening. Front Pharmacol 14:. https://doi.org/10.3389/fphar.2023.1298245

7. Zhang C, Peng K, Liu Q, et al (2024) Adavosertib and beyond: Biomarkers, drug combination and toxicity of WEE1 inhibitors. Crit. Rev. Oncol. Hematol. 193

8. Cole KA, Pal S, Kudgus RA, et al (2020) Phase I clinical trial of the WEe1 inhibitor adavosertib (AZD1775) with irinotecan in children with relapsed solid tumors: A COG phase I consortium report (ADVL1312). Clinical Cancer Research 26:1213–1219. https://doi.org/10.1158/1078-0432.CCR-19-3470

9. Matheson CJ, Backos DS, Reigan P (2016) Targeting WEE1 Kinase in Cancer. Trends Pharmacol. Sci. 37:872–881

10. Zhu JY, Cuellar RA, Berndt N, et al (2017) Structural Basis of Wee Kinases Functionality and Inactivation by Diverse Small Molecule Inhibitors. J Med Chem 60:7863–7875. https://doi.org/10.1021/acs.jmedchem.7b00996

11. Hirai H, Iwasawa Y, Okada M, et al (2009) Small-molecule inhibition of Wee1 kinase by MK-1775 selectively sensitizes p53-deficient tumor cells to DNA-damaging agents. Mol Cancer Ther 8:2992–3000. https://doi.org/10.1158/1535-7163.MCT-09-0463

12. Jameson NM, Kim D, Lee C, et al (2025) The Selective WEE1 Inhibitor Azenosertib Shows Synergistic Antitumor Activity with KRASG12C Inhibitors in Preclinical Models. Cancer Research Communications 5:240–252. https://doi.org/10.1158/2767-9764.CRC-24-0411

13. Oberoi A, Gonzalez Martin A, Jalving M, et al (2026) Debio 0123 (zedoresertib), a selective WEE1 inhibitor, in combination with car-boplatin in adult patients with platinum-resistant ovarian cancer: Expansion part of the Debio0123-101 phase 1 study

14. Zhang Z, Harish R, Elahi N, et al (2025) Targeting WEE1 Kinase for Breast Cancer Therapeutics: An Update. Int. J. Mol. Sci. 26

15. Squire CJ, Dickson JM, Ivanovic I, Baker EN (2005) Structure and inhibition of the human cell cycle checkpoint kinase, Wee1A kinase: An atypical tyrosine kinase with a key role in CDK1 regulation. Structure 13:541–550. https://doi.org/10.1016/j.str.2004.12.017

16. Kong A, Mehanna H (2023) WEE1 Inhibitor: Clinical Development. Curr Oncol Rep 23:107. https://doi.org/10.1007/s11912-021-01098-8/Published

17. Koh SB (2022) The expanding role of WEE1. Cell Signal 94:. https://doi.org/10.1016/j.cellsig.2022.110310

18. Du X, Li J, Luo X, et al (2020) Structure-activity relationships of Wee1 inhibitors: A review. Eur. J. Med. Chem. 203

19. Berman HM, Westbrook J, Feng Z, et al (2000) The Protein Data Bank

20. Word JM, Lovell SC, Richardson JS, Richardson DC (1999) Asparagine and Glutamine: Using Hydrogen Atom Contacts in the Choice of Side-chain Amide Orientation

21. Schrödinger (2023) Schrödinger Release 2023-3: MAESTRO

22. Lehtonen J V., Still DJ, Rantanen V V., et al (2004) BODIL: A molecular modeling environment for structure-function analysis and drug design. J Comput Aided Mol Des 18:401–419. https://doi.org/10.1007/s10822-004-3752-4

23. Sander T, Freyss J, Von Korff M, Rufener C (2015) DataWarrior: An open-source program for chemistry aware data visualization and analysis. J Chem Inf Model 55:460–473. https://doi.org/10.1021/ci500588j

24. Mysinger MM, Carchia M, Irwin JJ, Shoichet BK (2012) Directory of useful decoys, enhanced (DUD-E): Better ligands and decoys for better benchmarking. J Med Chem 55:6582–6594. https://doi.org/10.1021/jm300687e

25. Schrödinger L (2023) Schrödinger Release 2023-3: LigPrep

26. Harder E, Damm W, Maple J, et al (2016) OPLS3: A Force Field Providing Broad Coverage of Drug-like Small Molecules and Proteins. J Chem Theory Comput 12:281–296. https://doi.org/10.1021/acs.jctc.5b00864

27. Korb O, Stützle T, Exner TE (2009) Empirical scoring functions for advanced Protein-Ligand docking with PLANTS. J Chem Inf Model 49:84–96. https://doi.org/10.1021/ci800298z

28. Dixon SL, Smondyrev AM, Knoll EH, et al (2006) PHASE: A new engine for pharmacophore perception, 3D QSAR model development, and 3D database screening: 1. Methodology and preliminary results. J Comput Aided Mol Des 20:647–671. https://doi.org/10.1007/s10822-006-9087-6

29. Vainio MJ, Puranen JS, Johnson MS (2009) ShaEP: Molecular overlay based on shape and electrostatic potential. J Chem Inf Model 49:492–502. https://doi.org/10.1021/ci800315d

30. GraphPad Software (2024) GraphPad Prism (Version 10.4.1)

31. (2026) RDKit: Open-source cheminformatics

32. Schrödinger (2025) Schrödinger Release 2025-1: MAESTRO

Supplementary Files

This is a list of supplementary files associated with this preprint. Click to download.

- SupplementaryInformationcomplete.docx
- abstractfigure.tiff